Intermolecular potential and second virial coefficient of the water–hydrogen complex

Matthew P. Hodges[a)]
School of Chemistry, University of Birmingham, Edgbaston, Birmingham, B15 2TT, United Kingdom

Richard J. Wheatley
School of Chemistry, University of Nottingham, University Park, Nottingham, NG7 2RD, United Kingdom

Gregory K. Schenter
Chemical Sciences Division, Pacific Northwest National Laboratory, Richland, Washington 99352

Allan H. Harvey
Physical and Chemical Properties Division, National Institute of Standards and Technology, Boulder, Colorado 80305

(Received 8 September 2003; accepted 13 October 2003)

We construct a rigid-body (five-dimensional) potential-energy surface for the water–hydrogen complex using scaled perturbation theory (SPT). An analytic fit of this surface is obtained, and, using this, two minima are found. The global minimum has C_{2v} symmetry, with the hydrogen molecule acting as a proton donor to the oxygen atom on water. A local minimum with C_s symmetry has the hydrogen molecule acting as a proton acceptor to one of the hydrogen atoms on water, where the OH bond and H_2 are in a T-shaped configuration. The SPT global minimum is bound by 1097 μE_h ($E_h \approx 4.359\,744 \times 10^{-18}$ J). Our best estimate of the binding energy, from a complete basis set extrapolation of coupled-cluster calculations, is 1076.1 μE_h. The fitted surface is used to calculate the second cross virial coefficient over a wide temperature range (100–3000 K). Three complementary methods are used to quantify quantum statistical mechanical effects that become significant at low temperatures. We compare our results with experimental data, which are available over a smaller temperature range (230–700 K). Generally good agreement is found, but the experimental data are subject to larger uncertainties. © *2004 American Institute of Physics.*
[DOI: 10.1063/1.1630960]

I. INTRODUCTION

A detailed understanding of the thermodynamic properties of gas mixtures containing water is desirable for a number of reasons. The most important systems are moist air, where data can be used by industry and, perhaps more importantly, for metrology (e.g., for humidity standards), and combustion gases, such as from combustion turbines in the power industry. In these systems, the species whose interactions with H_2O need to be better understood are primarily linear molecules such as N_2, O_2, and CO_2.

In previous work, we developed accurate intermolecular potential-energy surfaces for water with helium[1] and with neon and argon.[2] This work demonstrated the ability of scaled perturbation theory to produce quantitatively accurate pair potentials with a reasonable computational effort. The resulting intermolecular potentials were used to compute temperature-dependent second cross virial coefficients $B_{12}(T)$ that have smaller uncertainties and cover a much wider temperature range than the values produced by experiment. This enables improved calculation of the thermodynamic properties of gaseous mixtures containing water. However, the monatomic gases considered previously are of limited practical importance. In this work, we take a further step toward the systems of greater interest by developing a potential-energy surface for the $H_2O\cdots H_2$ dimer. While we primarily view this system as a simpler (because of its fewer electrons) starting point from which to proceed to additional diatomic gases, vapor-phase mixtures of water and hydrogen are of some interest in their own right for certain types of fuel cells.[3] In addition, a recent review of B_{12} data for aqueous systems[4] specifically mentions the water–hydrogen system as one where better data are needed.

A number of *ab initio* studies on this system have been reported. These generally agree that the anisotropy of the potential-energy surface is dominated by the interaction of the permanent molecular electric multipole moments, and that this leads to two minima: one where the hydrogen molecule approaches the water molecule parallel to its C_{2v} axis, and on the oxygen side of the molecule; the other with the hydrogen molecule perpendicular to the plane of the water molecule, and forming a T-shaped configuration with an OH bond. The global minimum is the C_{2v} structure, with previous binding energies estimated in a range approximately spanning 700–1000 μE_h ($E_h \approx 4.359\,744 \times 10^{-18}$ J). One of the earlier studies, that by Schwenke *et al.*,[5] yielded one of the largest binding energies (about 950 μE_h), using a complete active space, self-consistent field (CASSCF) plus averaged coupled pair functional (ACPF) methodology, with a

a)Author to whom correspondence should be addressed. Electronic mail: matt@tc.bham.ac.uk.

$[5s4p2d1f/4s2p1d]$ basis set. The counterpoise correction procedure (CP) of Boys and Bernardi[6] was not applied, as the basis set superposition error (BSSE) was estimated to be small for the high-energy regions of the potential-energy surface of interest. However, the BSSE was reported to be about 0.1 kcal/mol (about 150 μE_h), near the van der Waals minimum, i.e., a significant fraction of the binding energy. Zhang *et al.*[7] used fourth-order Møller–Plesset perturbation theory to study the anisotropy of the potential-energy surface, and estimated the binding energy to be about 899 μE_h. A somewhat smaller estimate of about 738 μE_h was obtained by Balasubramanian *et al.*[8] at the CEPA(1) (coupled electron pair approximation) level of theory, whereas a fourth-order Møller–Plesset study by Phillips *et al.*[9] yielded a binding energy of about 916 μE_h, similar to the Zhang *et al.* value quoted above. A high-resolution mid-infrared observation of $H_2O\cdots H_2$ has recently been reported,[10] and it was concluded that large-amplitude motion occurs in this complex. Given a global potential energy surface that accurately describes this large-amplitude motion, it is possible to perform converged statistical mechanical sampling to obtain experimentally measurable quantities such as the second virial coefficient. Due to the light mass of the hydrogens in the system, one expects quantum statistical mechanical effects to become significant as the temperature is lowered. In the current work, we will determine the range of validity of approximate treatments of these effects. The structure of the rest of the paper is as follows: In Sec. II, we discuss the methods used to calculate and fit an analytic potential-energy surface for $H_2O\cdots H_2$, and the methods used to calculate the second virial coefficient. In Sec. III, we examine the form of the potential-energy surface, identifying important stationary points, and compare the second virial coefficient calculated from experimental data with that calculated from the fitted potential-energy surface. The conclusions from this work are drawn in Sec. IV.

II. METHODS

A. Coordinate system

The coordinate system used for $H_2O\cdots H_2$ is shown in Fig. 1. The H_2O molecule lies in the xz plane, with the origin at the oxygen atom, and the hydrogen atoms have $z<0$. The H_2 center-of-mass location is defined by the spherical polar coordinates, R, θ, and ϕ, and the orientation of H_2 by the spherical polar angles, θ' and ϕ'. The OH bond length and HOH bond angle are those recommended by Mas and Szalewicz,[11] i.e., $r_{OH}=1.8361\ a_0$ ($a_0\approx 0.052\,917\,72$ nm) and $\angle HOH=104.69°$; the H_2 bond length is $r_{HH}=1.449\ a_0$. These bond angles and bond lengths correspond to the molecules in their vibrational ground states. The H_2O geometry from Ref. 11 is derived from calculations, and the H_2 bond length is the experimentally determined value.

The angular coordinates are sampled using 256 entries in a four-dimensional Sobol sequence[12] in $\cos\theta$, ϕ, $\cos\theta'$, and ϕ' over the range $[0,\pi]$ for θ, θ', and ϕ', and $[0,\pi/2]$ for ϕ. The values of R sampled are 4, 5, 6, 7, 8, and 12 a_0, resulting in a total of 1536 points on the potential-energy surface.

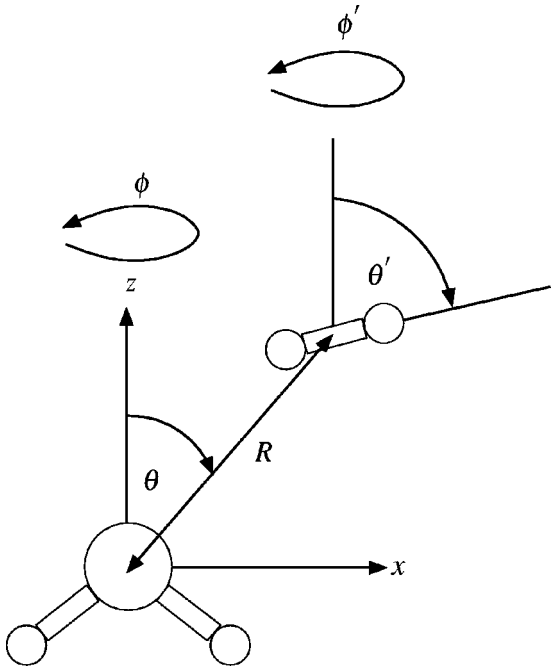

FIG. 1. Coordinate system used to describe the $H_2O\cdots H_2$ complex. The origin is at the oxygen atom, R, θ, and ϕ specify the H_2 center of mass, θ' and ϕ' the H_2 orientation.

B. Basis sets and *ab initio* calculations

We use modified versions of the augmented correlation-consistent (aug-cc-pVXZ) basis sets of Dunning and co-workers.[13,14] These ''shifted polarization'' (SP) variants are described elsewhere,[2,15,16] and involve shifting the Gaussian exponents of higher polarization functions (i.e., d and higher for hydrogen; f and higher for oxygen) to match the set of exponents of the polarization functions with lowest orbital angular momentum (i.e., p for hydrogen, and d for oxygen). This procedure has been shown to lead to improved dispersion-energy coefficients, and hence is useful for calculations on weakly bound systems. For the rest of this article, we refer to the aug-cc-pVXZ basis sets as AVXZ and the SP variants as SP-AVXZ.

The MOLPRO package[17,18] is used to perform supermolecule calculations, and the methods used are Hartree–Fock self-consistent field (SCF), second-order Møller–Plesset theory (MP2), and coupled cluster with single, double and perturbative triple substitutions [CCSD(T)]. Spherical basis functions, and the full counterpoise correction procedure of Boys and Bernardi[6] are used throughout.

Monomer charge densities for H_2O and H_2 are obtained with the SP-AVQZ basis sets at the SCF, MP2 and quadratic configuration interaction with single and double substitutions (QCISD) levels of theory. For the post-Hartree–Fock methods, the oxygen 1s orbital is frozen.

C. Scaled perturbation theory

At each point on the potential-energy surface described in Sec. II A, we calculate contributions to the interaction energy using the SP-AVQZ basis set. The contributions that

we include are first-order exchange-repulsion, first-order Coulomb, induction, dispersion, exchange-induction and exchange-dispersion,

$$\Delta E_{\rm int} = E_{\rm exch} + E_{\rm Coul} + E_{\rm ind} + E_{\rm disp} + E_{\rm exch\text{-}ind} + E_{\rm exch\text{-}disp}. \quad (1)$$

The framework we use is scaled perturbation theory (SPT), where, for some of the terms, the effects of intramolecular electron correlation effects are treated only approximately. This can be compared with the symmetry-adapted perturbation theory (SAPT) approach,[19] where, for each term, intramolecular electron correlation effects can be explicitly calculated, though with much greater computational expense. We now describe how we calculate the contributions to Eq. (1) term by term.

1. Exchange-repulsion energies

First-order exchange-repulsion energies are obtained from Heitler–London (HL) calculations, and intramolecular electron correlation effects are approximated using the following expression:

$$E_{\rm exch}^{\rm corr} \approx E_{\rm exch}^{\rm HL} \times \frac{S_\rho^{\rm corr}}{S_\rho^{\rm SCF}}, \quad (2)$$

where the S_ρ are the electronic charge-density overlap integrals, and "corr" represents a correlated level of theory. Equation (2) is based on the observation that the ratio of the exchange-repulsion and charge-density overlap integrals is insensitive to the level of theory at which it is calculated. This was first demonstrated for SCF and MP2 calculations for the water dimer,[20] and later for SCF and full configuration interaction (FCI) calculations for the helium dimer.[15] Here we introduce correlation effects by scaling the HL exchange-repulsion energies by the ratio of QCISD and SCF charge-density overlap integrals.

2. Coulomb energies

First-order Coulomb energies are calculated directly using the monomer charge densities obtained at the QCISD level of theory, using the SP-AVQZ basis sets,

$$E_{\rm Coul}^{\rm QCISD} = \int \rho_A^{\rm QCISD}(\boldsymbol{r}_A)\rho_B^{\rm QCISD}(\boldsymbol{r}_B) r_{AB}^{-1} {\rm d}\boldsymbol{r}_A {\rm d}\boldsymbol{r}_B, \quad (3)$$

where A and B represent H_2O and H_2.

3. Induction energies

Second-order coupled Hartree–Fock (CHF) induction energies are calculated directly, and scaled isotropically as follows. The long-range induction energy of H_2O is proportional to the product of the dipole polarizability (α) of H_2O and the square of the quadrupole moment (Θ) of H_2; the long-range induction energy of H_2 is proportional to the product of the dipole polarizability of H_2 and the square of the dipole moment (μ) of H_2O. SCF/SP-AVQZ values of $\alpha(H_2O)$, $\alpha(H_2)$, $\Theta(H_2)$, and $\mu(H_2O)$ are calculated, and the induction energies scaled using the ratio of accurate values from the literature and the SCF quantities, i.e.,

$$E_{\rm ind}(H_2O) = E_{\rm ind}^{\rm CHF}(H_2O) \times \frac{[\Theta(H_2)^2 \cdot \alpha(H_2O)]_{\rm lit}}{[\Theta(H_2)^2 \cdot \alpha(H_2O)]_{\rm SCF}}, \quad (4)$$

$$E_{\rm ind}(H_2) = E_{\rm ind}^{\rm CHF}(H_2) \times \frac{[\mu(H_2O)^2 \cdot \alpha(H_2)]_{\rm lit}}{[\mu(H_2O)^2 \cdot \alpha(H_2)]_{\rm SCF}}. \quad (5)$$

The accurate polarizabilities are calculated from dipole oscillator strength distribution (DOSD) data,[21] $\Theta(H_2)$ is taken from the work of Poll and Wolniewicz,[22] and $\mu(H_2O)$ from the CRC handbook.[23] This leads to scaling factors of 0.9409 and 0.8648 for the H_2O and H_2 induction energies, respectively.

4. Dispersion energies

Second-order time-dependent coupled Hartree–Fock (TDCHF) dispersion energies are calculated directly. The isotropic value of C_6 at this level of theory using the SP-AVQZ basis set is 22.0981 $E_{\rm h}\, a_0^6$, and the accurate DOSD value[21] is 23.21 $E_{\rm h}\, a_0^6$. Hence, we scale the TDCHF results isotropically by 1.050. The isotropic values of C_6 for the AVQZ and SP-AVQZ basis sets agree to within about 0.1% (both values being close to the Hartree–Fock limit), but the differences for the higher C_N, which make significant contributions to the interaction energies, are more marked: the SP-AVQZ values of C_8, C_{10}, and C_{12} are larger than the AVQZ values by about 4.2%, 20%, and 58%, respectively.

5. Exchange-induction energies

Exchange-induction energies are estimated by assuming the following breakdown of the SCF interaction energy:

$$\Delta E_{\rm SCF} \approx \Delta E_{\rm HL} + E_{\rm ind}^{\rm CHF} + E_{\rm exch\text{-}ind}^{\rm SCF}, \quad (6)$$

where $\Delta E_{\rm HL}$ is the sum of the first-order exchange-repulsion and Coulomb contributions, $E_{\rm ind}^{\rm CHF}$ the coupled Hartree–Fock induction energy, and $E_{\rm exch\text{-}ind}^{\rm SCF}$ the exchange-induction energy at the SCF level of theory. The exchange-induction contribution that we include in the total interaction energy [i.e., Eq. (1)] is an approximation of the MP2 contribution, and is obtained by scaling the SCF values by the ratio of MP2 and SCF charge-density overlap integrals. Hence we assume that intramolecular electron correlation effects can be incorporated into second-order exchange contributions in the same manner as for the first-order exchange [see Eq. (2)].

6. Exchange-dispersion energies

Like the exchange-induction energies, the exchange-dispersion energies are not calculated directly, but are estimated from supermolecule calculations, in this case at the MP2 level of theory. We use the following decomposition of the MP2 interaction energy:

$$\Delta E_{\rm MP2} \approx E_{\rm exch}^{\rm MP2} + E_{\rm Coul}^{\rm MP2} + E_{\rm ind}^{\rm MP2} + E_{\rm disp}^{\rm UCHF} + E_{\rm exch\text{-}ind}^{\rm MP2} + E_{\rm exch\text{-}disp}^{\rm MP2}. \quad (7)$$

To obtain $E_{\rm exch\text{-}disp}^{\rm MP2}$, which is used directly in Eq. (1), the exchange-repulsion energy is scaled according to Eq. (2), and the Coulomb energy is calculated directly from the MP2 monomer charge densities. The induction energy is the sum of the CHF components scaled by the ratio of the appropriate

monomer MP2 and SCF dipole polarizabilities. The uncoupled Hartree–Fock (UCHF) dispersion is a component of MP2 supermolecule interaction energies, and is calculated separately. The approximate MP2 exchange-induction energies are those described above.

7. Total interaction energies

To summarize, the total scaled perturbation theory interaction energies are composed of first-order exchange and Coulomb contributions at the QCISD level of theory, CHF induction, and TDCHF dispersion contributions scaled using monomer properties to give accurate asymptotic (multipolar) behavior, and second-order exchange-induction and exchange-dispersion at approximately the MP2 level of theory.

D. Fitting the potential-energy surface

The fitted $H_2O\cdots H_2$ potential is given by the function

$$\sum_{ab}\sum_{i}\sum_{jkl} C_{ab,i}^{jkl}(r_{ab})^{-i}(d_1)^j(d_2)^k(d_3)^l. \tag{8}$$

Here, a represents the five sites H_w, H_w', O, X, and X′ on the water molecule, and b represents the three sites H, H′, and Y on the hydrogen molecule. Sites X and X′ are in the plane of the H_2O molecule at 1 a_0 from the O nucleus and at half the tetrahedral angle (54.736°) from the water symmetry axis on the other side of the molecule from the hydrogens. Site Y is the center of the hydrogen molecule. r_{ab} is the distance from site a to site b, d_1 is the direction cosine $\hat{\boldsymbol{z}}_A\cdot\hat{\boldsymbol{R}}$, d_2 is the direction cosine $\hat{\boldsymbol{z}}_B\cdot\hat{\boldsymbol{R}}$, d_3 is the direction cosine $\hat{\boldsymbol{z}}_A\cdot\hat{\boldsymbol{z}}_B$. The unit vector $\hat{\boldsymbol{z}}_A$ points from the O atom along the water symmetry axis towards the center of the X and X′ sites, the unit vector $\hat{\boldsymbol{R}}$ points from O to Y, and the unit vector $\hat{\boldsymbol{z}}_B$ points along the H_2 axis from H′ to H. The fit uses 60 independent parameters, and minimizes the Boltzmann-weighted error,

$$W^2=\sum_g w_g\times(E_{\rm fit}(g)-E_{\rm calc}(g))^2 \Big/ \sum_g w_g, \tag{9}$$

where g represents the geometries, $E_{\rm fit}$ is the fitted function, $E_{\rm calc}$ is the calculated energy and the weights are given by

$$w_g=\exp[-(E_{\rm calc}(g)-E_0)/E_{\rm d}], \tag{10}$$

where $E_{\rm d}=3$ m$E_{\rm h}$ (about 950 K), and $E_0=-1000$ $\mu E_{\rm h}$. The weighting parameter $E_{\rm d}$ is chosen to ensure that repulsive configurations, accessible at the higher temperatures that we wish to consider, are given adequate weights in the fit, and will be represented accurately. The total weight for the fit is 884, and the error is $W\approx 9$ $\mu E_{\rm h}$. The parameters for the fitted potential-energy function and a FORTRAN subroutine to evaluate it are available as supplementary material via EPAPS.[24]

E. Second virial coefficients

1. Classical and semiclassical calculations

The classical component of the second virial coefficient is evaluated as the integral of the Mayer function over all space,

$$B_{\rm class}(T)=-\frac{1}{2}\int\langle\exp(-U_{12}/k_{\rm B}T)-1\rangle_{\Omega_1,\Omega_2}{\rm d}\boldsymbol{R}, \tag{11}$$

where U_{12} is the pair potential and $\langle\cdots\rangle_{\Omega_1,\Omega_2}$ represents averaging over all molecular orientations. Quantum effects can be introduced by using a semiclassical expansion in orders of $\hbar^2$ (see e.g., Gray and Gubbins[25]) and first-order translational and rotational corrections are given by

$$B_{\rm QM}^{\rm trans}(T)=\frac{\hbar^2}{24(k_{\rm B}T)^3}\times\frac{\langle\boldsymbol{F}^2\rangle_0}{2M_{\rm r}}, \tag{12}$$

$$B_{\rm QM}^{\rm rot}(T)=\frac{\hbar^2}{24(k_{\rm B}T)^3}\times\sum_{\alpha=x,y,z}\frac{\langle T_\alpha^2\rangle_0}{I_\alpha}, \tag{13}$$

where $\boldsymbol{F}$ is the force on each molecule, $M_{\rm r}$ is the reduced mass of the system, and T_α is the torque about the local molecular axis α with moment of inertia I_α. The $\langle\cdots\rangle_0$ notation represents integration weighted according to the zero-density pair distribution function. The rotational correction for this mixed system is the average of the two fragment contributions. The total first-order quantum-corrected second virial coefficient, $B_{\rm QM}^{(1)}(T)$, is defined as the sum of the contributions from Eqs. (11) to (13).

2. Path-integral calculations

An approach that uses the Feynman path-integral formalism for a fully quantum mechanical treatment of the second virial coefficient was introduced by Diep and Johnson.[26] In the current work, we follow the procedures that were shown to be successful in the calculation of the water–water second virial coefficient.[27] The expression for the quantum statistical mechanical second virial coefficient, $B_{\rm QM}(T)$, may be written as[26,27]

$$B_{\rm QM}(T)=-\frac{1}{2}\int{\rm d}\boldsymbol{R}\times\left\langle\exp\left(-\int_0^{\hbar\beta}{\rm d}\tau U[\boldsymbol{r}_1(\tau),\boldsymbol{r}_2(\tau),\Omega_1(\tau),\Omega_2(\tau)]/\hbar\right)-1\right\rangle_{\rm c}^{(0)}, \tag{14}$$

where the centroid constrained average, $\langle\cdots\rangle_{\rm c}^{(0)}$, is given by Feynman integration over periodic paths $\boldsymbol{r}_i(\tau+\hbar\beta)=\boldsymbol{r}_i(\tau)$ and $\Omega_i(\tau+\hbar\beta)=\Omega_i(\tau)$. Here, $\beta=1/k_{\rm B}T$ and $\boldsymbol{R}=\boldsymbol{r}_{1c}-\boldsymbol{r}_{2c}$, where

$$\langle\cdots\rangle_{\rm c}^{(0)}=\frac{1}{\rho_{\rm c}^{(0)}}\int D[\boldsymbol{r}_1(\tau)]D[\boldsymbol{r}_2(\tau)]D[\Omega_1(\tau)]D[\Omega_2(\tau)]\times\exp(-S_0/\hbar)\cdots\delta\left(\boldsymbol{r}_{1c}-\int_0^{\hbar\beta}\frac{{\rm d}\tau}{\hbar\beta}\boldsymbol{r}_1(\tau)\right)\times\delta\left(\boldsymbol{r}_{2c}-\int_0^{\hbar\beta}\frac{{\rm d}\tau}{\hbar\beta}\boldsymbol{r}_2(\tau)\right) \tag{15}$$

and the centroid density

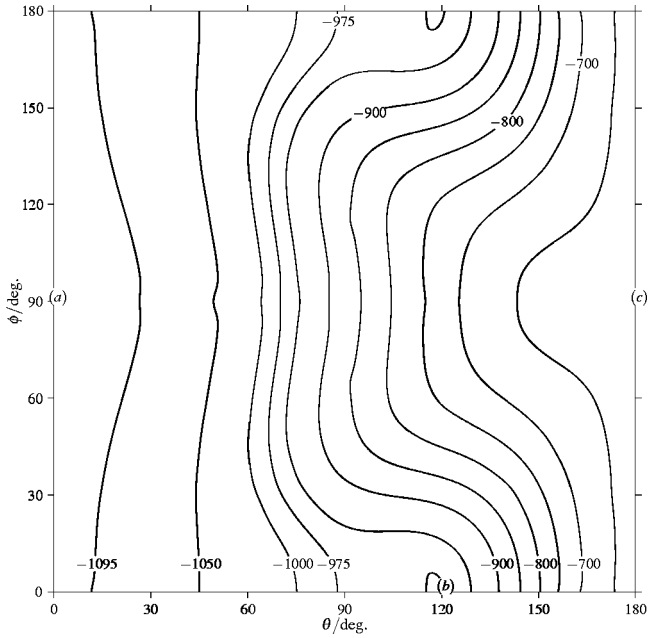

FIG. 2. Two-dimensional cut through the $H_2O\cdots H_2$ potential-energy surface. For each pair of θ and ϕ values, the energy is minimized with respect to R, θ' and ϕ'. The contours are given in μE_h.

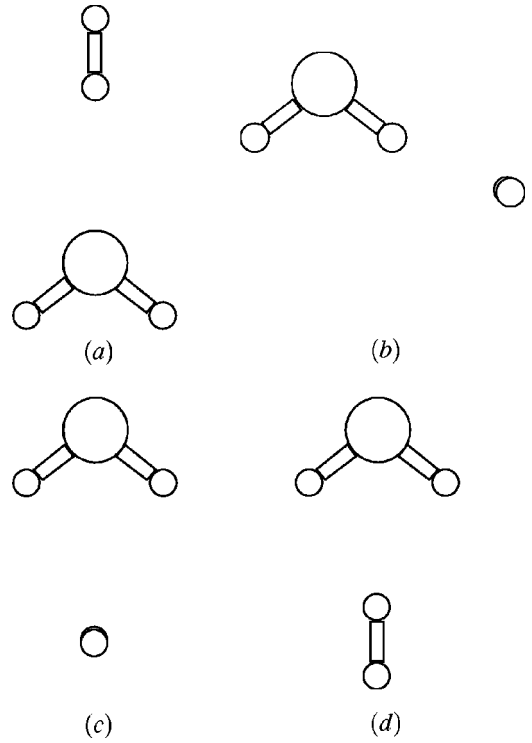

FIG. 3. Selected orientations of the $H_2O\cdots H_2$ complex for which cuts through the potential-energy surface, varying only R, are studied.

$$\rho_c^{(0)} = \int D[\mathbf{r}_1(\tau)]D[\mathbf{r}_2(\tau)]D[\Omega_1(\tau)]D[\Omega_2(\tau)] \times \exp(-S_0/\hbar)\,\delta\left(\mathbf{r}_{1c} - \int_0^{\hbar\beta} \frac{d\tau}{\hbar\beta}\mathbf{r}_1(\tau)\right) \times \delta\left(\mathbf{r}_{2c} - \int_0^{\hbar\beta} \frac{d\tau}{\hbar\beta}\mathbf{r}_2(\tau)\right). \quad (16)$$

The free Euclidian action, S_0, is given by

$$S_0 = \int_0^{\hbar\beta} d\tau \sum_{i=1}^{2} \left[\frac{1}{2}M_i\dot{\mathbf{r}}_i^2(\tau) + \frac{1}{2}\omega_i(\tau)\cdot\mathbf{I}_i\omega_i(\tau)\right], \quad (17)$$

where M_i is the total mass and $\mathbf{I}_i$ is the moment of inertia of each molecule, $\omega_i(\tau)$ is the angular velocity corresponding to dynamics in imaginary time, τ, and $\dot{\mathbf{r}}_i(\tau) = d\mathbf{r}_i(\tau)/d\tau$. Details of implementation and explicit expressions are given in Ref. 27.

3. Effective potential calculations

It was shown in previous work[27] that, for the case of the water–water interaction, an improved estimate of the second virial coefficient when compared with the first-order results of Eqs. (12) and (13) may be obtained from the semiclassical effective potential,

$$U_{12}^{(sc)} = U_{12} + \frac{\hbar^2\beta^2}{24}\sum_{i=1}^{2}\left[\frac{\mathbf{F}_i^2}{M_i} + \sum_{\alpha=x,y,z}\frac{T_{\alpha i}^2}{I_{\alpha i}}\right], \quad (18)$$

that replaces U_{12} in the classical expression to give

$$B_{QM}^{(sc)}(T) = -\frac{1}{2}\int \langle \exp(-U_{12}^{(sc)}/k_BT) - 1\rangle_{\Omega_1,\Omega_2} d\mathbf{R}. \quad (19)$$

$B_{QM}^{(sc)}$ and $B_{QM}^{(1)}$ are equal to order $\hbar^2$. In the sections to follow, we will compare results obtained from the $B_{QM}^{(sc)}$, $B_{QM}^{(1)}$ and the full B_{QM} expressions to obtain a consistent understanding of the low-temperature behavior of the second virial coefficient.

III. RESULTS

A. The potential-energy surface

We first examine the potential-energy surface by looking at a two-dimensional cut through it where, for values of θ and ϕ, we find the values of θ', ϕ', and R that minimize the potential energy. This surface is shown in Fig. 2, and gives the energy of the optimal position of H_2 for each line of approach towards H_2O. The global minimum, labeled (a), has H_2 on the oxygen side of H_2O, with the bond parallel to the C_{2v} axis (i.e., $\theta = \theta' = 0°$); R is about 5.67 a_0, and the interaction energy is very close to $-1100\ \mu E_h$, a value somewhat larger than estimated in previous studies.[5,7–9] The most significant improvement here is likely to be in the description of the dispersion interaction. In fact, the potential-energy surface is quite flat, and quite isotropic with respect to ϕ, at small θ, such that the region within 100 μE_h of the global minimum extends to about $\theta = 75°$ at $\phi = 0°$, and to about $\theta = 60°$ at $\phi = 90°$. A local minimum, labeled (b), has $\theta \approx 120°$ and $\phi = 0°$, i.e., the H_2 center of mass almost along the OH bond direction; the H_2 bond is perpendicular to the plane containing the H_2O molecule ($\theta' = \phi' = 90°$). This T-shaped configuration of the OH bond and the H_2 molecule has also been identified as a local minimum in previous studies (see above). The least favorable line of approach on the two-dimensional surface, labeled (c), has the H_2 center of

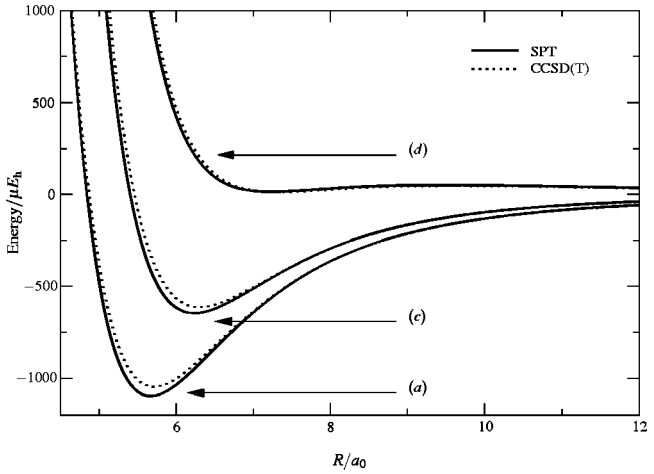

FIG. 4. Comparison of SPT and CCSD(T)/SP-AVQZ slices through the $H_2O\cdots H_2$ potential-energy surface. The configurations labeled (a), (c), and (d) are shown in Fig. 3.

mass on the H_2O C_{2v} axis on the hydrogen side of H_2O, and the H_2 orientation is the same as for (b); its minimum interaction energy is about -640 μE_h, at $R \approx 6.21$ a_0.

The orientations corresponding to the labeled stationary points are shown in Fig. 3, along with a fourth, labeled (d), which differs from (c) only in the H_2 orientation ($\theta' = 0°$). We show one-dimensional cuts (varying R, with all angular coordinates fixed) through the potential-energy surface in Fig. 4. The cuts are constructed by fitting a suitable functional form,

$$E_{\text{int}} \approx \exp[-\alpha(R-\rho)-\beta(R-\rho)^2] - \sum_{n=4,6,8} \frac{C_n}{R^n}, \qquad (20)$$

to discrete data, and these are shown for the energetically most and least favorable points on the two-dimensional surface discussed above [(a) and (c), respectively], and the orientation (d), where the interaction energy is always positive. The SPT curves are deeper than the corresponding CCSD(T)/SP-AVQZ ones for (a) and (c), and this reflects the fact that the scaling of the dispersion contribution, which is the major attractive part of the interaction energy, leads to a better description of this component than that recovered at the CCSD(T)/SP-AVQZ level of theory. The positions of the SPT minima are consequently at slightly smaller values of R [about 0.04, 0.07, and 0.08 a_0 for (a), (c), and (d), respectively] relative to the CCSD(T) values. We omit results for (b) here, since this cut is quite similar to (a); cut (d) is included to illustrate that the SPT model is capable of accurately describing regions of the potential-energy surface that are not strongly bound.

We present a breakdown of the interaction energy components from Eq. (1) for orientations (a), (c), and (d) at their optimal values of R, determined by minimizing Eq. (20), in Table I. The first-order Coulomb term is expected to be significantly more anisotropic than the dispersion term, and hence is expected to govern the relative stability of different molecular orientations (cf., the Buckingham–Fowler model[28]). The leading multipolar dipole-quadrupole term is given by[29]

$$\frac{\mu_A \Theta_B}{4\pi\varepsilon_0 R^4} \cdot \frac{3}{2}[\cos\theta_A(3\cos^2\theta_B - 1) - \sin\theta_A \sin 2\theta_B \cos\varphi], \qquad (21)$$

where $\varphi = \varphi_A - \varphi_B$, and θ_A, θ_B, φ_A and φ_B are Euler angles for molecules A and B with their centers of mass at Cartesian coordinates (0, 0, 0) and (0, 0, R). The angular factors from Eq. (21) are 3, 3/2, and -3 for orientations (a), (c), and (d), respectively. At the global minimum, the relative dipole–quadrupole orientations are optimal, and the first-order Coulomb and dispersion terms contribute similar amounts to the attractive part of the interaction; the induction and exchange-induction terms are somewhat less important, with a combined contribution of about 13% to the sum of the attractive interactions. The first-order exchange contributes nearly 90% of the total repulsive interaction, with the rest coming from the exchange-dispersion term. For (c), the dipole–quadrupole interaction is less favorable, and the dispersion term is the dominant attractive force, being about 30% larger in magnitude than the first-order Coulomb contribution. The induction energy contributes roughly the same proportion to the total attractive interaction as for (a), but the second-order exchange terms are much less significant, since the optimum value R is somewhat larger for (c), and these terms decay approximately exponentially. For (d), the first-order Coulomb term is large and positive, as expected from the above considerations, and at the shallow minimum, the interaction energy is about 14 μE_h.

1. Complete basis set limit extrapolation

To estimate the binding energy at the complete basis set (CBS) limit, we use the two-point extrapolation method of Halkier *et al.*[30] Interaction energies are calculated at the CCSD(T)/AVQZ and CCSD(T)/AV5Z levels of theory for orientation (a), which includes the global minimum (see Fig. 3), and a CCSD(T)/CBS estimate of the one-dimensional cut through the surface is obtained. An analytic

TABLE I. Minimum-energy positions, and breakdown of interaction energies into components, for the stationary points described in the text; see Eq. (1) and Fig. 3. The optimum separation, R_{min}, is given in a_0, and the energies in μE_h.

Label	R_{min}	Int	Exch	Coul	Ind	Disp	Exch-ind	Exch-disp
a	5.67	−1096.8	1574.9	−1337.6	−257.7	−1149.7	−126.6	199.8
c	6.23	−646.2	912.8	−642.9	−131.1	−818.4	8.2	25.3
d	7.22	13.9	216.6	249.3	−63.1	−384.9	−3.5	−0.3

fit of this cut is made using Eq. (20), and this yields an estimated CCSD(T)/CBS binding energy of 1076.1 μE_h, with $R_{min}=5.68\,a_0$. This is about 1% larger than the CCSD(T)/AV5Z binding energy, which is 1063.0 μE_h ($R_{min}=5.69\,a_0$), and about 2% smaller than the SPT value.

2. Effect of H_2 bond length

The rotational temperature of H_2 is about 85 K, so at the higher limit of the temperature range of interest here ($T \approx 2000$ K), a significant number of rotational states will be occupied. The vibrational temperature of H_2 is about 6000 K, so in contrast, only the ground vibrational state will have a significant population.

We calculate the H_2 potential-energy curve at the FCI level of theory using an aug-cc-pV6Z basis set, for $0.5 \leqslant R_{HH} \leqslant 3.0\,a_0$, and fit an analytic function to accurately represent these data. We then solve the one-dimensional nuclear Schrödinger equation using the Fourier Grid Hamiltonian method,[31] for a number of rotational energy levels, labeled J. This is done by adding the centrifugal potential,

$$V_{rot}(R_{HH})=\hbar^2 J(J+1)/(2M_r R_{HH}^2), \tag{22}$$

to the fitted function. Here, M_r is the reduced mass, calculated from the mass of the hydrogen atom (1.00794 atomic mass units). For $J=0$, the expectation value of R_{HH} for the vibrational ground state is $1.4486\,a_0$, in agreement with the reported experimental value of $1.449\,a_0$. The expectation value of the quadrupole moment is 0.482764 a.u., which can be compared with the accurate Poll and Wolniewicz[22] value of 0.483 535 a.u. The expectation value of the polarizability is 5.411 953 a.u., in good agreement with the DOSD value of 5.427 922 a.u.,[21] and the accurate value calculated by Rychlewski[32] of 5.417 04 a.u.

At 1000 K, the Boltzmann-weighted average over the populated rotational states of the expectation value of R_{HH} is $1.4634\,a_0$, i.e., 1.0% larger than the value at 0 K. At 2000 K, this is increased to $1.4756\,a_0$, i.e., 1.9% larger. The quadrupole moment is larger relative to the rotational ground state value by 1.6% and 3.0% at 1000 and 2000 K, respectively, whereas the corresponding increases for the polarizability are 1.2% and 2.2%. The C_{2v} minimum at the CCSD(T)/SP-AVQZ level of theory with $R_{HH}=1.463\,a_0$ has a binding energy of 1062 μE_h, compared to 1047 μE_h for $R_{HH}=1.449\,a_0$. Hence, the correction to the binding energy at 1000 K associated with the stretched H_2 bond is about half the size of that associated with using a finite basis set (see above).

A similar calculation for H_2O would be quite complex. However, it seems likely that the effect of the rotation of H_2O on the pair potential would be small based on the fact that measured dipole moments for H_2O in higher rotational states up to $J=6$ (Ref. 33) differ by less than 1% from the dipole moment in the ground state.[34]

The corrections associated with using a finite basis set, and the H_2 stretching, increase the binding energy of the $H_2O\cdots H_2$ complex relative to the CCSD(T)/SP-AVQZ value corresponding to 0 K. Taking these into account, we estimate that the SPT method is in error by no more than 5%, placing the binding energy in the range of about 1050–1150 μE_h.

TABLE II. $H_2O\cdots H_2$ second virial coefficients derived from experimental data. Temperatures are given in K, B_{12} and their uncertainties ΔB_{12} in $cm^3\,mol^{-1}$.

T	B_{12}	ΔB_{12}	Reference
233.16	−47.8	75.1	36
243.16	−51.9	27.4	36
243.16	−0.2	48.4	35
253.15	−13.2	15.4	36
253.15	−1.7	18.3	35
263.15	−15.1	14.2	36
263.15	−3.2	10.9	35
271.15	−3.7	14.1	35
273.15	−30.0	14.7	36
283.16	−64.7	9.3	37
293.16	−68.0	10.0	37
310.92	−10.6	5.3	38
366.46	2.1	6.2	38
422.00	9.4	8.9	38
477.55	11.5	16.0	38
653.15	4.0	12.8	40
673.15	2.9	15.8	40
693.15	1.7	10.1	40
713.15	1.1	10.7	40

We use this assessment of the accuracy of the SPT method to estimate uncertainties in the calculated values of $B_{12}(T)$ below.

B. Second virial coefficients

1. Experiment

B_{12} may be obtained from measurements of the H_2O mole fraction in hydrogen gas equilibrated with ice[35,36] or with liquid water.[37,38] The procedures for deriving B_{12} from these data and estimating its uncertainty have been described previously;[1,2] the results are given in Table II. The uncertainties in Table II (standard uncertainty with coverage factor 2) reflect only the measurement of water content in the gas phase; additional factors such as neglect of higher virial coefficients are not included. The solubility of hydrogen in liquid water is calculated from the Henry's constants recommended in Young[39] for the data of Kosyakov *et al.*;[37] for the data of Gillespie and Wilson,[38] the measured coexisting liquid compositions are used.

Seward *et al.*[40] made volumetric measurements of several $H_2O\cdots H_2$ mixtures at high temperatures. They reported mixture second virial coefficients, B_m, which are rigorously related to the pure-component and cross virial coefficients by

$$B_m=x_1^2 B_{11}+2x_1x_2B_{12}+x_2^2B_{22}, \tag{23}$$

where x is the mole fraction and subscripts 1 and 2 represent water and hydrogen, respectively.

At each experimental composition, the measured B_m can be combined with known values of B_{11} and B_{22} to yield B_{12}. Unfortunately, this produces values of B_{12} with much scatter, especially at the ends of the composition range. This is not surprising; Eubank and Hall[41] have shown that (for equal uncertainties in B_{11} and B_{22}, which is approximately the case here) an equimolar mixture produces the most reliable values of B_{12} from Eq. (23), with the uncertainty growing at more asymmetric compositions. We therefore average only

TABLE III. Values of $\phi_{12}=B_{12}-T(dB_{12}/dT)$ for $H_2O\cdots H_2$ derived from vapor-phase enthalpy-of-mixing data. Temperatures are given in K, ϕ_{12} and their uncertainties $\Delta\phi_{12}$ in $cm^3\,mol^{-1}$.

T	ϕ_{12}	$\Delta\phi_{12}$	Reference
373.17	−35	12	43
378.17	−25	19	43
383.17	−11	17	43
393.17	−8	13	43
403.17	−16	18	43
413.17	−2	8	43
423.16	−7	15	43
448.2	−35.3	61	44
473.2	−25.7	51	44
498.2	−38.8	31	44
523.2	12.7	21	44
548.2	35.2	19	44
573.2	39.7	15	44
598.2	24.3	11	44
648.2	14.8	11	44
698.2	7.8	17	44

the values for $x_2=0.25$, 0.4, 0.6, and 0.8, with the 0.4 and 0.6 compositions given double weight. The results are given in Table II, where the uncertainties reflect the scatter of values obtained at different compositions.

Finally, vapor-phase enthalpy-of-mixing data can, when extrapolated to low pressure, yield $\phi_{12}=B_{12}-T(dB_{12}/dT)$. At temperatures from approximately 373 to 423 K, values of ϕ_{12} were reported by Smith *et al.*[42] and later reanalyzed by Wormald and Lancaster.[43] In Table III, we give the values from their reanalysis, along with their reported uncertainties.

At higher temperatures and pressures, excess enthalpies for water–hydrogen mixtures were reported by Lancaster and Wormald,[44] superseding earlier measurements.[45] As described previously for the water–argon system,[2] we extrapolate these data to zero pressure in order to extract ϕ_{12}. Those values are also given in Table III. As was the case for water–argon, the uncertainties in these values of ϕ_{12} result primarily from our estimate of the uncertainty in the zero-pressure extrapolation.

In the calculations described in this section, $B(T)$ for pure hydrogen is required. Since no precise representation existed, we fit an equation to the data of Michels *et al.*,[46] which extend to approximately 423 K. Above that temperature, we use values of $B(T)$ calculated from the corrected *ab initio* potential of Diep and Johnson.[26,47] The resulting equation is

$$B(T)=\sum_{i=1}^{4} c_i(T^*)^{d_i}, \tag{24}$$

where $T^*=T/100$ K, B and the c_i have units of $cm^3\,mol^{-1}$, and the values of c_i and d_i are given in Table IV.

$B(T)$ for pure water is also required. In previous work,[1,2] we used the correlation of Hill and McMillan[48] for this purpose. However, the upper temperature limit of this correlation is only 573 K, not high enough for the data of Seward *et al.*[40] or for some of the data of Lancaster and Wormald.[44] We therefore use a new correlation[49] that covers the entire temperature range required. The effect of changing the $B(T)$ correlation for water is always much less than the overall uncertainty in the data for both B_{12} in Table II and ϕ_{12} in Table III.[50]

TABLE IV. Parameters for an analytic approximation of $B(T)$ for H_2. The c_i are in $cm^3\,mol^{-1}$ and the d_i are dimensionless. The analytic form is given in Eq. (24).

i	c_i	d_i
1	42.0803	−0.33
2	−143.982	−1.4
3	146.918	−1.8
4	−47.5601	−2.2

2. Theory

The classical, first-order semiclassical, effective-potential, and path-integral results for $B_{12}(T)$ have been calculated using the fitted SPT potential-energy surface. For Eqs. (11)–(13) radial quadrature out to 45 a_0 with a step size 0.01 a_0 is used, and the angular degrees of freedom are sampled using a Sobol sequence of 16 384 (i.e., 2^{14}) entries. We estimate that the errors due to the sampling are of the order of 0.1 $cm^3\,mol^{-1}$ at 100 K and reduced to about 0.01 $cm^3\,mol^{-1}$ at 1000 K. Calculations are performed over a temperature range of 100–3000 K.

To evaluate the exact quantum statistical mechanical expression for the second virial coefficient given by Eq. (14), we express the path in terms of P discretizations. Details of the explicit form of the discretization are contained in Ref. 27. Metropolis Monte Carlo sampling is carried out along a mesh in the center-of-mass distance, R. Along this mesh, we evaluate the effective Mayer function, $\exp(-V_{\rm eff}(R)/k_{\rm B}T)-1$, or, equivalently, the effective potential, $V_{\rm eff}(R)$. The exact quantum statistical mechanical second virial coefficient is given by

$$B(T)=-2\pi\int_0^\infty(\exp(-V_{\rm eff}(R)/k_{\rm B}T)-1)R^2dR. \tag{25}$$

We consider four temperatures, 100, 150, 200 K, and 250 K. For the temperatures of 200 and 250 K, we consider $P=5$ and $P=10$. No significant changes are observed when sampling with the large discretization. For the temperatures of 100 and 150 K, we consider $P=10$ and $P=20$. Again, no significant changes when compared to the statistical uncertainties are observed when we sample with the larger discretization. For all temperatures, we sample 10^6 Monte Carlo moves with a step in R of 0.05 nm over a range of 0.3 nm $\leqslant R\leqslant$ 0.6 nm to recover the shape of the effective Mayer function. In the important region of 0.3 nm$\leqslant R\leqslant$0.4 nm, where the effective Mayer function has a peak, we perform 10^7 Monte Carlo moves with a step in R of 0.005 nm. By collecting these results, we are able to create a smooth interpolation of the effective Mayer function by scaling our calculation of the semiclassical effective potential. This allows us to do the integration in R and obtain a consistent value for B. We confirm that the error due to this fitting procedure is insignificant compared to the statistical error of the Monte

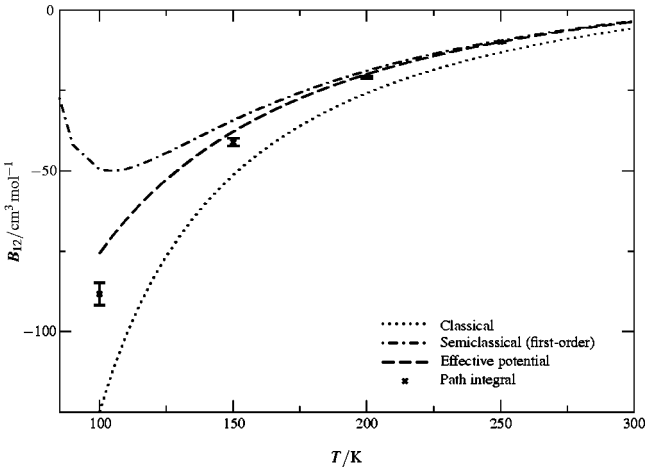

FIG. 5. A comparison of different theoretical methods used to calculate the second virial coefficient of the $H_2O\cdots H_2$ complex.

Carlo sampling. Error estimates are obtained by propagating over the integration the statistical error from Monte Carlo evaluation of the effective Mayer function.

Comparison of B_{12} for the different computational methods is shown in Fig. 5. The first-order semiclassical results are a reasonable approximation to the path-integral results at higher temperatures; for example, at 250 K, the difference is about 0.5 cm^3 mol^{-1}, and the estimated uncertainty in the path-integral result is about 0.2 cm^3 mol^{-1}. However, close to 100 K, the gradient of the first-order results is qualitatively incorrect, and B_{12} increases at temperatures lower than this, becoming large and positive by 50 K. Results from the various methods of calculating B_{12} are collected in Table V, including the rotational and translational contributions from the first-order approximation. Not surprisingly, the majority of the first-order correction arises from the rotational terms, in particular that associated with the motion of H_2, and this method cannot be considered useful for this system at temperatures lower than about 150 K. At 250 K, where the first-order method is quite accurate, the sum of the rotational terms is about twice as large as the translational contribution. At temperatures below 150 K, the first-order expression fails to recover the qualitative trend with temperature. The results from the effective potential recover the qualitative trend, but significant deviations from the exact converged path-integral results still occur at 150 K. At temperatures above 200 K, the methods become consistent with one another, and for temperatures where experimental measurements have been made, results obtained from the first-order expression are appropriate.

TABLE VI. Parameters for analytic approximation of $B_{12}(T)$ for the $H_2O\cdots H_2$ complex. The c_i are in cm^3 mol^{-1} and the d_i are dimensionless. The analytic form is that given in Eq. (24).

i	c_i	d_i
1	33.047	−0.21
2	−250.41	−1.50
3	285.42	−2.26
4	−186.78	−3.21

An analytic fit is constructed to represent $B_{12}(T)$. For this purpose, the first-order perturbation results are used at high temperatures, the effective potential results are used from 250 to 500 K, and path-integral values are used at 100, 150, 200, and 250 K. The same expression used above for H_2 [Eq. (24)] is used; Table VI gives the fitted parameters. Equation (24) can be differentiated with respect to T to yield $\phi_{12}(T)$.

This fit is recommended for use from 200 to 2000 K; in this range the errors in the fit are less than those associated with the numerical evaluation of $B_{12}(T)$. The fit is constrained to behave reasonably outside this temperature range, but significant extrapolation is not recommended, especially in the low-temperature direction. With the functional form of Eq. (24), we were unable to fit the path-integral points at 100 and 150 K within their uncertainties, even with the addition of more terms. This suggests that a different functional form might be required to reproduce low-temperature values of $B(T)$ in systems with large quantum effects; we did not attempt to find such a form in this work because of the lack of practical interest in these lowest temperatures for this system.

In Table VII, we list values of B_{12} for the $H_2O\cdots H_2$ complex generated from Eq. (24) at specific temperatures with the parameters given in Table VI. Table VII also gives the uncertainties in B_{12}; these are based on first-order calculations using SPT potentials with binding energies increased and decreased by 5% (see Sec. III A).

3. Comparison with experimental data

The best theoretical results (i.e., the fit using the parameters in Table VI) are compared with the experimental data

TABLE V. Calculated second virial coefficients for $H_2O\cdots H_2$. Classical, first-order quantum-corrected, effective-potential, and path-integral results are shown, calculated with the fitted SPT potential-energy surface. The translational and rotational components of the first-order results are shown, as are the estimated uncertainties, σ, in the path-integral results. The temperatures are given in K, and the B_{12} in cm^3 mol^{-1}.

		First-order					Path integral	
T	Classical	Total	Rot.(H_2O)	Rot.(H_2)	Trans.	Effective potential	Total	σ
100	−125.0	−49.61	9.515	52.02	13.81	−75.65	−88.26	3.5
150	−51.34	−34.31	2.081	10.97	3.984	−37.81	−41.13	1.2
200	−25.85	−18.92	0.8124	4.140	1.986	−19.96	−20.91	0.42
250	−13.17	−9.472	0.4149	2.045	1.242	−9.92	−9.92	0.18

TABLE VII. $H_2O\cdots H_2$ second virial coefficients derived using Eq. (24) and the parameters from Table VI. Temperatures are given in K, B_{12} and their uncertainties ΔB_{12} in $cm^3\ mol^{-1}$.

T	B_{12}	ΔB_{12}
200	−20.56	3.37
250	−9.96	2.61
300	−3.61	2.11
400	3.66	1.51
500	7.62	1.16
600	10.03	0.94
700	11.59	0.79
800	12.65	0.69
900	13.39	0.61
1000	13.91	0.55
1200	14.56	0.46
1400	14.90	0.40
1600	15.07	0.36
1800	15.13	0.33
2000	15.13	0.31

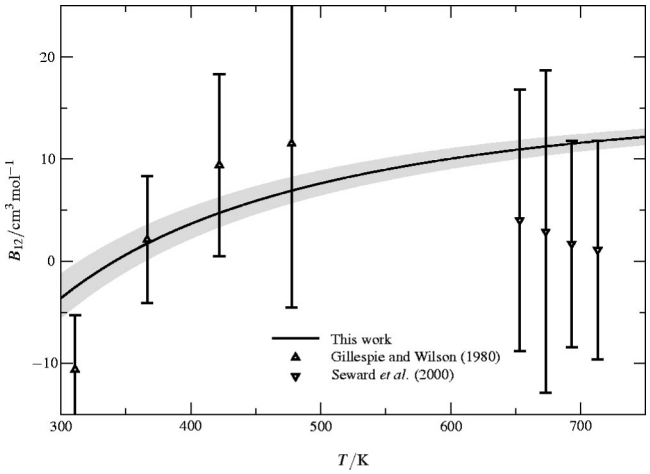

FIG. 7. A comparison of theoretical and experimental second virial coefficient data for the $H_2O\cdots H_2$ complex; higher temperature range. An estimate of the uncertainty in this work is indicated by the shaded region.

from Table II in Figs. 6 and 7. Our results are generally consistent with the data, with the exception of the measurements of Kosyakov *et al.*[37] Data from this laboratory for the water–argon system also deviate significantly from our previous calculations and from other experimental data from several sources;[2] it therefore seems likely that these data are not reliable (a recent compilation of B_{12} data[4] reached the same conclusion). The high-temperature data of Seward *et al.*[40] look as if they may be systematically too low, but are consistent with our values within their uncertainties.

Figure 8 shows our results for $\phi_{12}(T)$, along with the experimental data of Wormald and coworkers from Table III. The agreement is reasonable with the exception of three points between approximately 550 and 600 K. The large positive values of ϕ_{12} (larger than the values of B_{12}) derived from the data of Lancaster and Wormald[44] in this region implies a significantly negative value of dB_{12}/dT, which is physically unrealistic at these temperatures. It is interesting that the older measurements on this system from Wormald and Colling,[45] which were supposedly superseded by the data listed in Table III, are in significantly better agreement with our calculations at these three temperatures. As for the $B_{12}(T)$ results, our calculations lead to significantly smaller error estimates than those for the experimental data.

IV. CONCLUSIONS

We use scaled perturbation theory to examine the potential-energy surface of $H_2O\cdots H_2$, with basis sets chosen to give a good description of the dispersion interaction. The binding energy is found to be about 1100 μE_h, and the first-order Coulomb and second-order dispersion contributions are of similar magnitude at the global minimum. However, the anisotropy of the first-order Coulomb energy is much greater than for the dispersion term, and it is repulsive for some relative orientations of the two molecules. Good agreement is seen between the scaled perturbation theory and accurate coupled-cluster calculations for both strongly bound and repulsive regions of the potential-energy surface.

The second virial coefficient, $B_{12}(T)$, is calculated using an analytic fit of the potential-energy surface. Quantum ef-

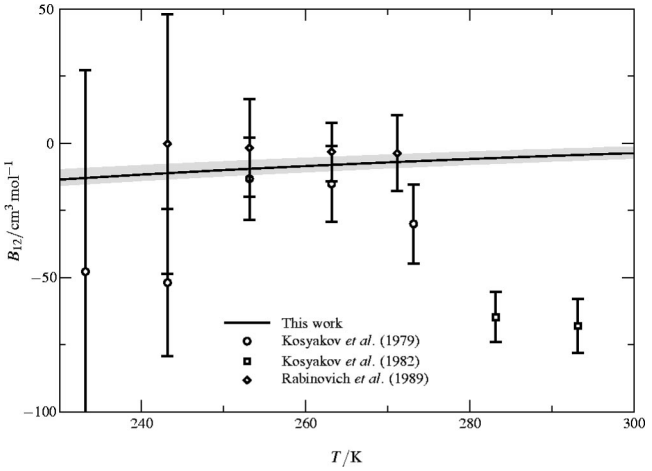

FIG. 6. A comparison of theoretical and experimental second virial coefficient data for the $H_2O\cdots H_2$ complex; lower temperature range. An estimate of the uncertainty in this work is indicated by the shaded region.

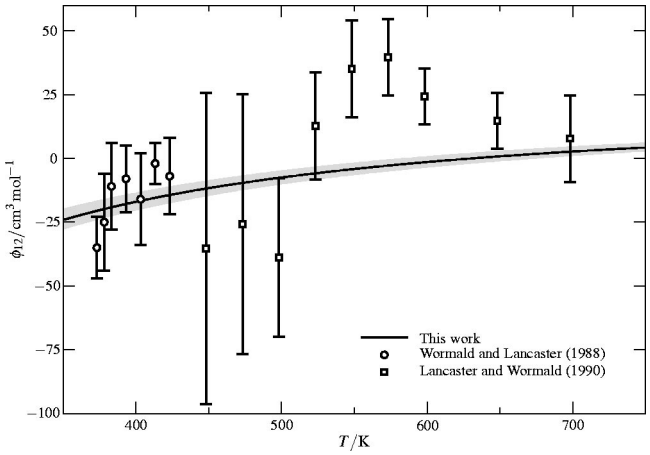

FIG. 8. A comparison of theoretical and experimental $\phi_{12}=B_{12}-T(dB_{12}/dT)$ data for the $H_2O\cdots H_2$ complex. An estimate of the uncertainty in this work is indicated by the shaded region.

fects are included using several methodologies. Classical, semiclassical (to first order in $\hbar^2$), effective-potential, and path-integral calculations are performed, and results are presented for a temperature range of 100–3000 K. The semiclassical results are reliable for temperatures greater than about 250 K, whereas the effective-potential results are reasonable even at 150 K. The estimated uncertainty in the path-integral calculations at 100 K is significantly smaller than the error associated with the effective potential results. Experimental values of B_{12} are extracted from a number of sources. They are mostly consistent with our calculations, but have large uncertainties and are available over a smaller temperature range, about 200–700 K, than needed for the applications of interest to us. We fit an analytic function to $B_{12}(T)$ and calculate $\phi_{12}=B_{12}-T(\mathrm{d}B_{12}/\mathrm{d}T)$, for which experimental data are also available. Again, the theoretical results are generally consistent with the data, but have smaller uncertainties.

We conclude that, for this system, where the range of experimental thermodynamic data and the accuracy of values for B_{12} extracted from these data leave much to be desired, a theoretical approach is preferable. Furthermore, the scaled perturbation theory presented here involves no adjustable parameters and offers an efficient way of calculating interaction energies for weakly bound complexes. We expect the same to be true for the interactions of water with the diatomic gases N_2 and O_2, which are of greater practical interest.

ACKNOWLEDGMENTS

This work was funded in part by the Engineering and Physical Sciences Research Council. One of us (G.K.S.) was supported by the Division of Chemical Sciences, Office of Basic Energy Sciences, U.S. Department of Energy. Battelle operates the Pacific Northwest National Laboratory for the Department of Energy. The authors thank E. W. Lemmon for assistance in fitting $B(T)$ correlations.

[1] M. P. Hodges, R. J. Wheatley, and A. H. Harvey, J. Chem. Phys. **116**, 1397 (2002).
[2] M. P. Hodges, R. J. Wheatley, and A. H. Harvey, J. Chem. Phys. **117**, 7169 (2002).
[3] V. Gurau, H. Liu, and S. Kakac, AIChE J. **44**, 2410 (1998).
[4] A. V. Plyasunov and E. L. Shock, J. Chem. Eng. Data **48**, 808 (2003).
[5] D. W. Schwenke, S. P. Walch, and P. R. Taylor, J. Chem. Phys. **94**, 2986 (1991).
[6] S. F. Boys and F. Bernardi, Mol. Phys. **19**, 553 (1970).
[7] Q. Zhang, L. Chenyang, Y. Ma, F. Fish, M. M. Szczęśniak, and V. Buch, J. Chem. Phys. **96**, 6039 (1992).
[8] V. Balasubramanian, G. G. Balint-Kurti, and J. H. van Lenthe, J. Chem. Soc., Faraday Trans. **89**, 2239 (1993).
[9] T. R. Phillips, S. Maluendes, A. D. McLean, and S. Green, J. Chem. Phys. **101**, 5824 (1994).
[10] M. J. Weida and D. J. Nesbitt, J. Chem. Phys. **110**, 156 (1999).
[11] E. M. Mas and K. Szalewicz, J. Chem. Phys. **104**, 7606 (1996).
[12] *The GNU Scientific Library*, Version 1.1.1, http://sources.redhat.com/gsl/ (2002).
[13] T. H. Dunning, J. Chem. Phys. **90**, 1007 (1989).
[14] D. E. Woon and T. H. Dunning, J. Chem. Phys. **98**, 1358 (1993).
[15] M. P. Hodges and R. J. Wheatley, J. Mol. Struct.: THEOCHEM **591**, 67 (2002).
[16] M. P. Hodges, E. Bichoutskaia, A. S. Tulegenov, and R. J. Wheatley, Int. J. Quantum Chem. (to be published).
[17] H.-J. Werner, P. J. Knowles, R. D. Amos *et al.*, MOLPRO, a package of *ab initio* programs (University of Birmingham, United Kingdom, 1997).
[18] Certain commercial products are identified in this paper, but only in order to adequately specify the procedure. Such identification neither constitutes nor implies recommendation or endorsement by either the U.S. government or the National Institute of Standards and Technology.
[19] B. Jeziorski, R. Moszynski, and K. Szalewicz, Chem. Rev. (Washington, D.C.) **94**, 1887 (1994).
[20] M. P. Hodges and R. J. Wheatley, Chem. Phys. Lett. **326**, 263 (2000).
[21] D. J. Margoliash and W. J. Meath, J. Chem. Phys. **68**, 1426 (1978).
[22] J. D. Poll and L. Wolniewicz, J. Chem. Phys. **68**, 3053 (1978).
[23] *CRC Handbook of Physics and Chemistry*, 75th ed. edited by D. R. Lide (CRC Press, Boca Raton, 1995).
[24] See EPAPS Document No. E-JCPSA6-120-002402 for the source code and compilation instructions for the FORTRAN subroutine described in the journal article. A direct link to this document may be found in the online article's HTML reference section. The document may also be reached via the EPAPS homepage (http://www.aip.org/pubservs/epaps.html) or from ftp.aip.org in the directory/epaps. See the EPAPS homepage for more information.
[25] C. G. Gray and K. E. Gubbins, *Theory of Molecular Fluids* (Clarendon, Oxford, 1984), Vol. 1.
[26] P. Diep and J. K. Johnson, J. Chem. Phys. **112**, 4465 (2000).
[27] G. K. Schenter, J. Chem. Phys. **117**, 6573 (2002).
[28] A. D. Buckingham and P. W. Fowler, J. Chem. Phys. **79**, 6426 (1983).
[29] A. J. Stone, *The Theory of Intermolecular Forces* (Oxford University Press, Oxford, 1996).
[30] A. Halkier, W. Klopper, T. Helgaker, P. Jørgensen, and P. R. Taylor, J. Chem. Phys. **111**, 9157 (1999).
[31] C. C. Marston and G. G. Balint-Kurti, J. Chem. Phys. **91**, 3571 (1989).
[32] J. Rychlewski, Mol. Phys. **41**, 833 (1980).
[33] S. A. Clough, Y. Beers, G. P. Klein, and L. S. Rothman, J. Chem. Phys. **59**, 2254 (1973).
[34] S. L. Shostak, W. L. Ebenstein, and J. S. Muenter, J. Chem. Phys. **94**, 5875 (1991).
[35] V. A. Rabinovich, V. G. Beketov, and M. B. Iomtev, Tables of the National Standard Reference Data Service of the USSR, Technical Report No. R348-89, All-Union Research Institute of Technical Information, Archival Deposit No. 615, Moscow, 1989, cited in V. A. Rabinovich and V. G. Beketov, *Moist Gases: Thermodynamic Properties* (Begell House, New York, 1995).
[36] N. E. Kosyakov, B. I. Ivchenko, and P. P. Krishtopa, J. Appl. Chem. USSR **52**, 881 (1979).
[37] N. E. Kosyakov, B. I. Ivchenko, and P. P. Krishtopa, Vopr. Khim. i Khim. Tekhnol. **68**, 33 (1982).
[38] P. C. Gillespie and G. M. Wilson, GPA Research Report RR-41, Gas Processors Association, Tulsa, OK, 1980.
[39] *Hydrogen and Deuterium*, Vol. 5/6 in IUPAC Solubility Data Series, edited by C. L. Young (Pergamon, Oxford, 1981).
[40] T. M. Seward, O. M. Suleimenov, and E. U. Franck, in *Steam, Water, and Hydrothermal Systems: Physics and Chemistry Meeting the Needs of Industry*, edited by P. R. Tremaine, P. G. Hill, D. E. Irish, and P. V. Balakrishnan, in *Proceedings of the 13th International Conference on the Properties of Water and Steam* (NRC Research Press, Ottawa, 2000), p. 104.
[41] P. T. Eubank and K. R. Hall, AIChE J. **36**, 1661 (1990).
[42] G. Smith, A. Sellars, T. K. Yerlett, and C. J. Wormald, J. Chem. Thermodyn. **15**, 29 (1983).
[43] C. J. Wormald and N. M. Lancaster, J. Chem. Soc., Faraday Trans. **84**, 3141 (1988).
[44] N. M. Lancaster and C. J. Wormald, J. Chem. Eng. Data **35**, 11 (1990).
[45] C. J. Wormald and C. N. Colling, J. Chem. Thermodyn. **17**, 437 (1985).
[46] A. Michels, W. de Graaf, and C. A. ten Seldam, Physica (Amsterdam) **26**, 393 (1960).
[47] P. Diep and J. K. Johnson, J. Chem. Phys. **113**, 3480 (2000).
[48] P. G. Hill and R. D. C. MacMillan, Ind. Eng. Chem. Res. **27**, 874 (1988).
[49] A. H. Harvey and E. W. Lemmon, J. Phys. Chem. Ref. Data (to be published).
[50] This was also the case when the analysis reported in earlier work (Refs. 1, 2) was repeated with the new correlation for water's $B(T)$. The largest changes were in the high-temperature values of ϕ_{12} in Table VI of Ref. 2 (those from Ref. 39 in that paper), where the revised analysis produces values of ϕ_{12} that are less negative by about 1 or 2 $\mathrm{cm^3\,mol^{-1}}$.